Commun Nonlinear Sci Numer Simulat 65 (2018) 248–259

Contents lists available at ScienceDirect

Commun Nonlinear Sci Numer Simulat

journal homepage: www.elsevier.com/locate/cnsns

Research paper

Ensemble separation and stickiness influence in a driven stadium-like billiard: A Lyapunov exponents analysis

Matheus S. Palmero[a,*], André L.P. Livorati[a,b], Iberê L. Caldas[c], Edson D. Leonel[a,d]

[a] Departamento de Física, UNESP - Universidade Estadual Paulista, Av. 24A, 1515, Bela Vista, Rio Claro, SP 13506-900, Brazil
[b] School of Mathematics, University of Bristol, Bristol BS8 1TW, United Kingdom
[c] Instituto de Física, IFUSP - Universidade de São Paulo, Rua do Matão, Tr.R 187, Cidade Universitária, São Paulo, SP 05314-970, Brazil
[d] Abdus Salam International Center for Theoretical Physics, Strada Costiera 11, Trieste 34151, Italy

ARTICLE INFO

Article history:
Received 10 January 2018
Revised 12 May 2018
Accepted 25 May 2018
Available online 28 May 2018

ABSTRACT

The dynamics of an ensemble of non-interacting particles suffering elastic collisions inside a driven stadium-like billiard is investigated through a four-dimensional nonlinear mapping. The system presents a resonance velocity, which plays an important role on the ensemble separation according to the initial velocities. The idea is to use the Lyapunov exponents to study the ensemble separation. We compare two different methods: (i) Finite Time Lyapunov Exponents and (ii) Wolf Linearization Algorithm. Results from both methods show good agreement regarding the separation of ensembles. Our results give support for the fact that stickiness influences the dynamics providing a crucial effect in the ensemble separation of the velocities for the time-dependent stadium-like billiard.

1. Introduction

The modelling of dynamical systems has received special attention of the scientific community in the last decades [1–4]. Models that present mixed phase space with chaotic seas, invariant tori and stability islands are of special interest. This is due to the presence of nonlinear phenomenon such as stickiness [3–7], which is described as orbits that get trapped around a stability island for a finite time, sometimes very long. Moreover such systems present a variety of rich and interesting non-linear phenomena. This includes anomalous transport and diffusion [5,6], bifurcations in non-equilibrium systems [8], shrimp-like structures in the parameter space [9], crisis between manifolds and attractors [10] among many others. It is worth to mention that some of these nonlinear phenomena have their nature not yet fully understood, therefore giving rise to many open problems.

A billiard is within a class of dynamical systems of particular interest. It is defined by the dynamics of a particle (billiard ball), which in the absence of external fields, moves along straight lines inside a closed domain (billiard table). The notion of billiards is known since Birkhoff [11] proposed the investigation of a problem for the dynamics of a point-like particle moving along geodesic line inside a closed domain, experiencing collisions with the boundaries. After the Birkhoff's work, Sinai [12], Bunimovich [13,14] and Gallavotti [15] had also made important contributions giving mathematical support to the field. Since then, several applications have been found in different areas of research including optics [16], quantum dots [17], microwaves [18], astronomy [19] and laser dynamics [20].

* Corresponding author.
E-mail address: palmero@usp.br (M.S. Palmero).

https://doi.org/10.1016/j.cnsns.2018.05.024
1007-5704/

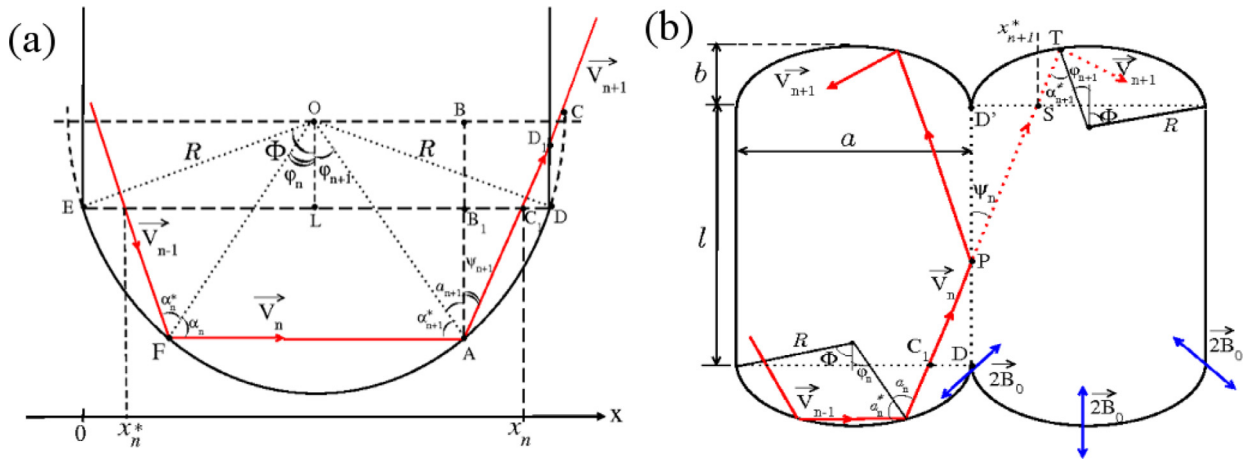

Fig. 1. An illustration of the stadium-like billiard with its dynamical variables and parameters. In (a) an illustration of the successive collisions. In (b) an illustration of the indirect collisions.

It was Bunimovich [21] who introduced a billiard with the shape of a football stadium. The original stadium billiard boundary consists of two parallel straight lines connected with two semi-circular arcs. In 1999, Loskutov and coauthors [22] introduced a stadium-like billiard, where the concave boundary could be parabolic [23–25] or just a circumference segment [24,25]. They also considered the dynamics with a time-dependent boundary [26] proposing a conjecture about the unlimited diffusion of the velocity of the particle, known as Loskutov–Ryabov–Akinshin (LRA) conjecture. The conjecture says that if a billiard has any chaotic component in its static boundary version, the introduction of a time perturbation in the boundary is a sufficient condition for the dynamics exhibits unlimited diffusion in the velocity known as Fermi acceleration (FA) [27].

In this paper we investigate the dynamics of a driven stadium-like billiard seeking to understand and describe the behaviour of the ensemble separation of particles. Our original contribution to this study is to make the investigation by using the Lyapunov exponents. For some combination of control parameters, the system presents a resonance between orbits that rotate around period-1 fixed points and the external boundary perturbation. This resonance sets a critical velocity V_r, where particles with initial velocities above V_r exhibit FA [24–26], on the other hand, particles with initial velocities below V_r exhibit a decay of energy as time evolves. The decay of energy is also thanks to the influence of stickiness phenomenon [28]. Statistically the critical resonance velocity acts like a ensemble separation, or as a Maxwell's Demon [29]. The Lyapunov exponent analysis provides another description of this ensemble separation and, it was done considering two different numerical methods: (i) the Finite Time Lyapunov Exponent (FTLE) [30,31] and (ii) the Wolf Linearization Algorithm [32]. Both analysis show a good agreement regarding the separation of ensembles via the Lyapunov exponents analysis.

This paper is organized as following: In Section 2 we describe the dynamics of the stadium billiard and setup a brief scenario for the resonance and the ensemble separation. Section 3 is devoted to present the numerical methods used to calculate the Lyapunov exponents for both ensembles, explaining how the methods agree to describe the ensemble separation, also giving emphasis to the stickiness influence. Finally in Section 4 we draw some final remarks and conclusions of this study.

2. The stadium-like billiard and chaotic properties

The stadium-like billiard describes the dynamics of a point-like particle experiencing collisions with time-dependent boundaries $\partial Q = \partial Q(t)$, where ∂Q has the shape of a stadium, as show Fig. 1. The description is the non-dissipative version where collisions between the particle and the boundary are elastic. There are two distinct situations for the dynamics of a particle inside this billiard: (i) successive collisions and (ii) indirect collisions. For case (i) the particle has successive collisions with the same focusing component. On the other hand, in (ii), after a collision with a focusing boundary, the next collision of the particle is with the opposite one. The particle can, in principle, collides many more times with the parallel borders. To attenuate this particular orbit, we use the so called unfolding method [23,33] since the billiard has an axial symmetry. The time-dependence on the boundary was considered only in the focusing components and introduced via a periodic function of the type $R(t) = R_0 + r\sin(wt)$, where $R_0 \gg r$. Thus velocity of the boundary is then obtained by

$$\dot{R}(t) = B(t) = B_0\cos(wt), \tag{1}$$

with $B_0 = rw$ and r is the amplitude of oscillation of the moving boundary while $w = 1$ is the frequency of oscillation. In our approach, the dynamics of the model is described in the static wall approximation, in the sense that the boundary is assumed to be fixed, but at the moment of the collisions, it exchanges energy and momentum with the particle as if the boundary were normally moving. See Ref. [34] for a discussion of the 1-D Fermi accelerator model.

2.1. Mapping

The dynamics is given by the variables $(\alpha_n, \phi_n, t_n, V_n)$, where α is the angle between the trajectory of the particle and the normal line at the collision point, ϕ is the angle between the normal line at the collision point and the vertical line in the symmetry axis, V is the velocity of the particle and t is the time at the instant of the impact. The index n denotes the nth collision of the particle with the boundary. As an initial condition we assume that, at the initial time $t = t_n$, the particle is at the focusing boundary and the velocity vector directs towards to the billiard table. As a notation, all starred variables are measured immediately before the collision. Fig. 1(a) shows an illustration of a trajectory with successive collisions, where $R = (a^2 + 4b^2)/(8b)$ and $\Phi = \arcsin(a/2R)$. The control parameters a, b and l are also displayed in the figure.

Let us consider case (i) first. The condition $|\phi_{n+1}| \leq \Phi$ warrants a successive collision and it is modelled by the following recurrence relations

$$\begin{cases} \alpha^*_{n+1} = \alpha_n \\ \phi_{n+1} = \phi_n + \pi - 2\alpha_n \pmod{2\pi} \\ t_{n+1} = t_n + \dfrac{2R\cos(\alpha_n)}{V_n} \end{cases} . \tag{2}$$

If $|\phi_{n_1}| > \Phi$, then case (ii) applies, and the particle collides with the opposite focusing component and we use the unfolding method [23,33] to describe the dynamics. Two auxiliary variables are introduced in this case namely, ψ, which is the angle between the vertical line at the collision point and the particle trajectory, and x, representing the projection over the horizontal axis. A schematic illustration of the indirect collisions are shown in Fig. 1(b) yielding the following recurrence relations

$$\begin{cases} \psi_n = \alpha_n - \phi_n \\ x_n = \dfrac{R}{\cos(\psi_n)}[\sin(\alpha_n) + \sin(\Phi - \psi_n)] \\ x_{n+1} = x_n + l\tan(\psi_n) \\ \alpha^*_{n+1} = \arcsin[\sin(\psi_n + \Phi) - x_{n+1}\cos(\psi_n)/R] \\ \phi_{n+1} = \psi_n - \alpha^*_{n+1} \\ t_{n+1} = t_n + \dfrac{R[\cos(\phi_n) + \cos(\phi_{n+1}) - 2\cos(\Phi)] + l}{V_n\cos(\psi_n)} \end{cases} . \tag{3}$$

For both cases (i) and (ii), the recurrence relations for the final velocity V_{n+1} and the angle α_n are the same. The expression for V_{n+1} is given by

$$V_{n+1} = \sqrt{V_n^2 + 4B_n^2 + 4V_nB_n\cos(\alpha^*_n)} \ . \tag{4}$$

Using Snell's law, the reflection angle α_n is given by

$$\alpha_n = \arcsin\left(\frac{|\vec{V_n}|}{|\vec{V_{n+1}}|}\sin(\alpha^*_n)\right) \ . \tag{5}$$

The dynamics is described by Eqs. (2)–(5). For the specific steps and geometrical procedures used for the mapping obtainment check Refs. [24–26,29].

2.2. Resonance critical velocity

The resonance phenomenon is typical of dynamical system which presents mixed phase space. In action-angle variables, the rotation number around the period-1 orbit is given by $\sigma = \arccos\left(1 - \frac{8bl}{a^2\cos^2(\psi^*_n)}\right)$, where $\psi^*_n = \arctan(\frac{ma}{l})$ is the fixed point [23–25], with $m \geq 1$ representing the number of mirrored stadiums that the particle traverses in a trajectory by considering the unfolding method.

Considering now a trajectory whose orbit moves around a period-1 fixed point in the static version of the billiard (with no time-dependent boundaries) the time spent between two successive collisions is $\tau \approx \frac{l}{\cos(\psi^*_n)V_n}$ [24,25]. Thus the rotation period of this orbit around the fixed point is $T_{rot} = \frac{2\pi\tau}{\sigma}$.

When time perturbation is introduced in the focusing boundaries, it has an external perturbation period as $T_{ext} = \frac{2\pi}{w}$. If $T_{rot} = T_{ext}$ we have a resonance between the oscillation of the moving boundaries and the rotation orbits around the fixed points. After some rearrangement we find the resonance velocity as

$$V_r = \frac{wl}{\cos(\psi^*_n)\arccos\left(1 - \frac{8bl}{a^2\cos^2(\psi^*_n)}\right)} \ . \tag{6}$$

Eq. (6) is valid when the defocussing mechanism is not active in the dynamics, which restricts the range of the control parameters a, b and l [23]. It was shown that depending of the point ψ^*, orbits with low initial velocity can get trapped on specific island in the phase space [28].

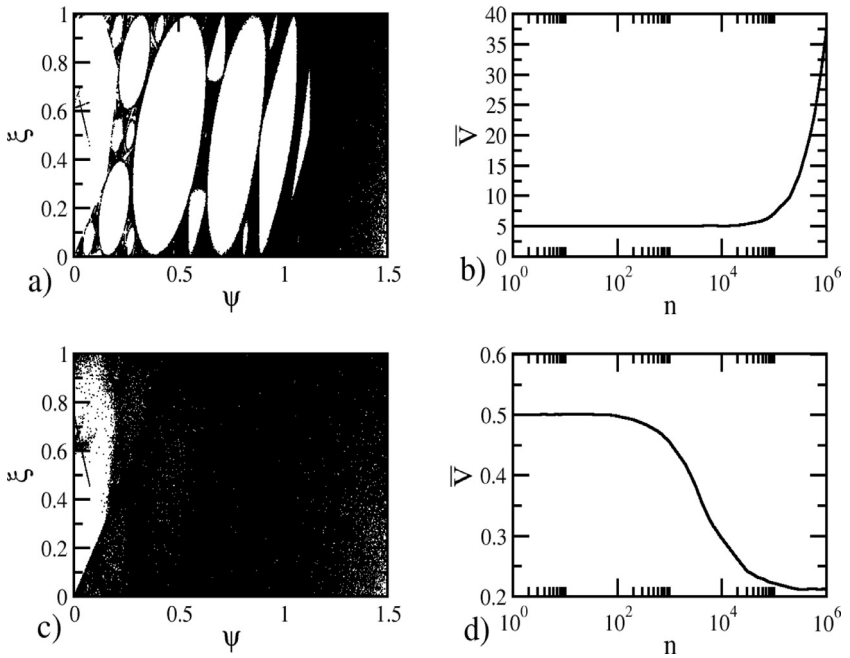

Fig. 2. (a) and (b) show the phase space and the behaviour of the average velocity for initial velocity $V_0 = 5.0$. The regime of Fermi acceleration is easily recognized. The same in (c) and (d), however with $V_0 = 0.5$ and the decay of average velocity can be observed. For both simulations the numerical value for the resonant velocity is $V_r \cong 1.2$.

2.3. Ensemble separation

The resonance velocity separates the dynamics in two different behaviours. The separation occurs according to the initial velocity of a particle inside of the stadium-like billiard. For initial velocity larger than the resonance one, the average velocity of a particle rises leading to FA. However, for initial velocity smaller than the resonance, the average velocity of a particle decreases. The decay of the average velocity leads to a decay of energy in the system therefore separating the ensembles in a high and low energy.

With the introduction of the time perturbation, the invariant curves surrounding the fixed points become porous. They behave in a similar way to a stochastic layer [35–37]. As a consequence, the whole phase space becomes accessible for the particle. An orbit initially in the chaotic sea may penetrate in the vicinity of a stability island. For this particular case, stickiness acts together with the resonance, where orbits that get trapped around stability islands, have more chances to change their behaviour [28].

According to the previously subsection, Eq. (6) gives us a value for the resonant velocity, and that depends on the control parameters of the stadium billiard. Thus, for the parameters $l = 1$, $a = 0.5$, $b = 0.01$, and $m = 1$, the resonant velocity is $V_r \cong 1.2$. The behaviour of the dynamics is strongly dependent on the initial velocity of the particles as shown in Fig. 2. In Fig. 2(a) and (b) we have high initial velocity ensemble. One can see that the phase space has well defined stability islands among a chaotic sea. The average velocity grows as a function of n. On the other hand, Fig. 2(c) and (d) show the low initial velocity ensemble where the whole phase space is now accessible for a single orbit. For large times the average velocity tends to decay reaching a constant plateau for sufficiently long time, settling the dynamics in a region of the phase space that correspond to a periodic island in the static boundary dynamics [28].

The phase space of the time-dependent stadium billiard can also be constructed using the angular coordinates ϕ and α, or else using the auxiliary variables ξ and ψ [24,25], where ξ is given by $\xi = \frac{1}{2} + \frac{R_0 \sin(\phi_{n+1})}{a}$ and is modulated by the unity. The statistical properties are unaltered. In the next section we discuss the ensemble separation by calculating the Lyapunov exponents for the driven stadium-like billiard.

3. Lyapunov exponents

The Lyapunov exponent is an important tool and has been widely used to quantify the average expansion or contraction rate for a small volume of initial conditions [4]. The stability of an orbit, called x_n, can be set through the evolution of a neighbour (satellite) orbit to x_n, named $x_n{}'$. Both orbits are separated by an infinitesimal distance δx_n, where $\delta x_n(0) = x_n{}'(0) - x_n(0)$, and the zero index refers to the initial time or iteration, depending on the continuum or discrete spectrum.

For chaotic orbits, the distance grows exponentially with time, according to

$$\delta x_n \propto \delta x_n(0) e^{\lambda n} \ , \tag{7}$$

where λ is the local exponential expansion rate. Thus we define a parameter to characterize how chaotic a given orbit is, such as

$$\lambda = \lim_{n\to\infty} \lim_{\delta x_n(0)\to 0} \frac{1}{n} \ln\left(\frac{|\delta x_n|}{|\delta x_n(0)|}\right) . \tag{8}$$

Here, λ is a quantity responsible to estimate the average exponential separation rate between the original orbit and its satellite one, known as Lyapunov exponent. If the Lyapunov exponent is positive the trajectory shows sensibility to the initial conditions and the orbit is said to be chaotic. A non-positive Lyapunov exponent indicates regularity and the dynamics can be periodic or quasi-periodic.

In this section we discuss some aspects of the dynamics of the driven stadium-like billiard via Lyapunov exponents, using two distinct numerical methods. We evaluate the dynamics for both ensemble of velocities: the higher one ($V_0 > V_r$), where FA is inherent, and the lower one ($V_0 < V_r$), where stickiness ally with resonance, creates a trapping mechanism, that does not allow FA in the system [28]. We chose to use the finite time Lyapunov exponents (FTLE) technique and the Wolf linearization algorithm as well.

3.1. Finite Time Lyapunov Exponents (FTLE)

For a N-dimensional map, one usually calculates N distinct FTLEs by employing the Benettin algorithm [38,39]. The principle to obtain the Lyapunov exponents is to verify if two very close orbits diverge exponentially, in average, from each other as time evolves. However, the consideration of $t \to \infty$ in Eq. (8) is not feasible. Therefore we truncate the time evolution at a finite time, but long. The numerical procedure is setup as follows: given an initial original orbit (α_0, ϕ_0, V_0, t_0) and a satellite orbit (α_0', ϕ_0', V_0', t_0'), we evolve both orbits according the mapping dynamics, and after a defined finite time (ℓ), we measure the distance between them as

$$\delta_\ell = \sqrt{(\Delta V)^2 + (\Delta t)^2 + (\Delta\alpha)^2 + (\Delta\phi)^2} \ , \tag{9}$$

where $\Delta V = V_\ell - V_\ell'$, $\Delta t = t_\ell - t_\ell'$, $\Delta\alpha = \alpha_\ell - \alpha_\ell'$ and $\Delta\phi = \phi_\ell - \phi_\ell'$. The distance between the orbits δ_ℓ is used to rescale the satellite orbit to the same direction of the original orbit. After that, the same procedure is restarted. The rescaled values for the satellite orbit are given by

$$\begin{cases} \alpha_0' = \alpha_\ell + [\delta_0(\alpha_\ell' - \alpha_\ell)]/\delta_\ell \\ \phi_0' = \phi_\ell + [\delta_0(\phi_\ell' - \phi_\ell)]/\delta_\ell \\ V_0' = V_\ell + [\delta_0(V_\ell' - V_\ell)]/\delta_\ell \\ t_0' = t_\ell + [\delta_0(t_\ell' - t_\ell)]/\delta_\ell \end{cases} , \tag{10}$$

where δ_0 is the initial difference between the orbits set as $\delta_0 = 10^{-10}$. The FTLE is then computed considering n successive ℓ time intervals, until the finite time predetermined is reached, according the following expression

$$\lambda_\ell = \frac{1}{n\ell} \sum_{j=1}^{n} \ln\left(\frac{\delta_j}{\delta_0}\right) . \tag{11}$$

It is important to notice that the Eq. (11) defines the largest FTLE for the system.

In the dynamics of the driven stadium-like billiard chaotic and regular motion can coexist in the phase space. Such coexistence introduces large variations and local instability along a reference chaotic trajectory. These variations are related to alternations between different types of motion. In order investigate such alternations, we used the Finite-Time Lyapunov Exponent (FTLE) [30,31,38,39]. Once the trappings caused by orbits in stickiness regime happen just for a finite time, this technique is useful to quantify the trapping effects. It was shown [30,31] that when the FTLE distributions present small values, it is related to existence of long-lived jets from a two-dimensional model for fluid mixing and transport. This can be understood as stickiness trajectories in the phase space.

Choosing an initial conditions set up in the chaotic sea as $\alpha_0 = 1.5$ and $\varphi_0 = 0$, we obtain a distribution of the FTLE called $h(\lambda)$. The fluctuations of λ are responsible for the increase of the shape and height of $h(\lambda)$. Due to different dynamics observed in the driven stadium-like billiard, the value of λ and its distribution $h(\lambda)$ have high dependence to the initial conditions. In these cases, $h(\lambda)$ are a mix of Gaussian distribution with long tails and primary peaks near zero, which indicate stickiness in the dynamics.

Fig. 3 shows a comparison between the FTLE, its distribution $h(\lambda)$ and the phase space for the same orbit used in the FTLE, considering both ensembles of energy. For all panels of Fig. 3 we used step-size of $\ell = 100$. Such value was tested empirically and agreed to be convenient to visualize the trappings caused by stickiness. Initially Fig. 3(a) and (b) show the evolution of the FTLE for a single orbit in the chaotic sea considering the low and high ensemble respectively, and in Fig. 3(c) and (d) display its distribution.

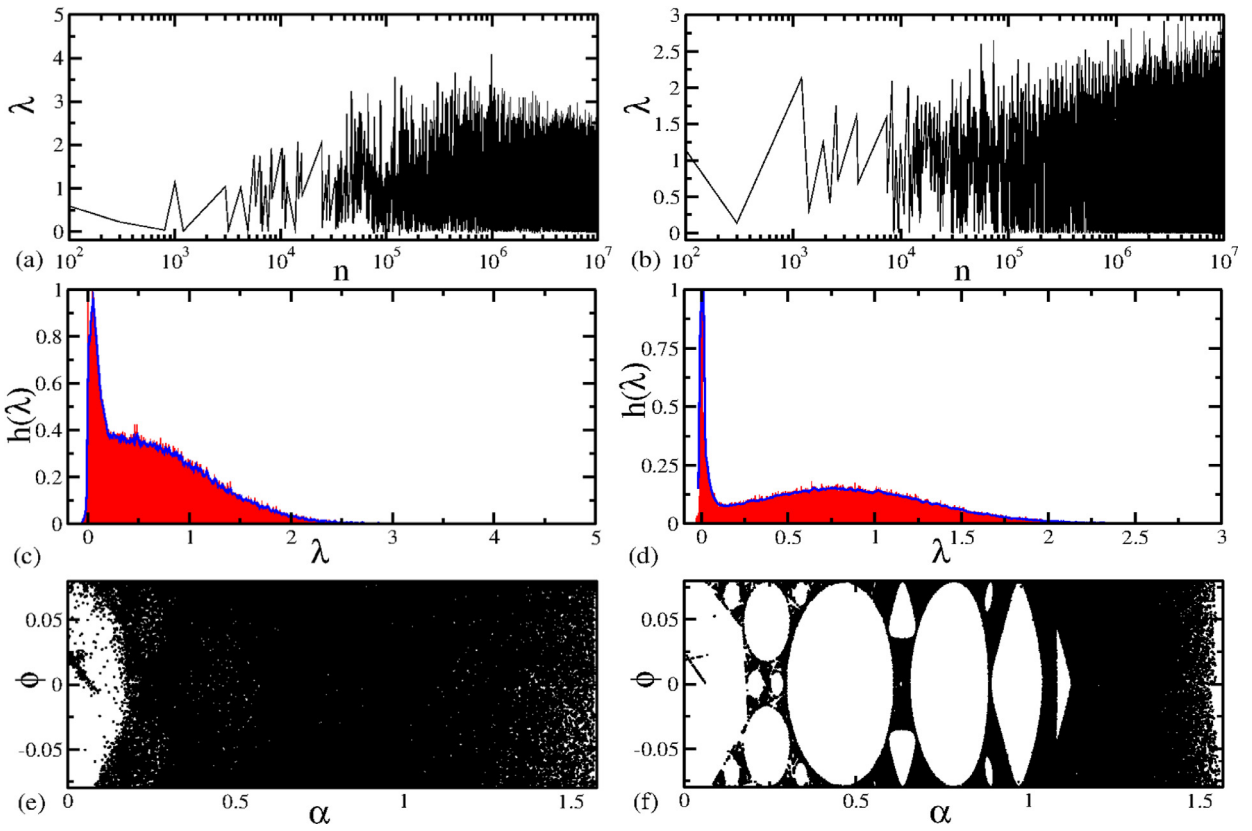

Fig. 3. Comparison between the FTLE, its distribution and the phase space for both energy ensembles. In (a), (c) and (e), the lower energy ensemble is shown. The orbit goes to a stationary state for long times thanks to the stickiness influence allied with resonance. The FTLE describes well this behaviour. And, in (b), (d) and (f) the high energy ensemble is represented where FA in inherent. Stickiness is not influencing the dynamics as indicated in (d) by the primary peak near zero in $h(\lambda)$, but the chaotic behaviour also plays its part, creating a secondary peak in a Gaussian-like shape. In all items of this Figure, we used a step size for time intervals as $\ell = 100$.

In Fig. 3(a), (c) and (e) we have the low energy ensemble for an initial velocity $V_0 = 0.6$. Here, the orbits have a tendency to reach stationary state, thanks to the action of resonance allied with stickiness effect. Indeed, the FTLE confirms such a tendency in Fig. 3(a), where for long times and considering the average, it reaches a plateau near zero. Its distribution in Fig. 3(c), displays distinct peaks near zero value and a monotonically decay. According to $h(\lambda)$, the FTLE assumes many times zero values, therefore mimicking a stable behaviour.

On the other hand, in Fig. 3(b),(d) and (f) we have the high energy ensemble for an initial velocity $V_0 = 6$. In this scenario the dynamics exhibits unlimited velocity growth, characteristic of Fermi acceleration [28,29]. Fig. 3(d) shows a primary peak near zero in $h(\lambda)$, which also indicates the presence of stickiness in the dynamics. However we have a better shaped distribution along a secondary peak, where a Gaussian-like distribution may be fitted.

Moreover, for the high energy ensemble, the phase space depicted in Fig. 3(f) shows a smaller portion of chaotic sea in comparison to the low energy ensemble in Fig. 3(e). Then, a carefully look on the numerical values for the FTLEs shows that, for the decaying regime, the values of λ are higher than FA regime, as expected.

Finally, in order to check the robustness of these results for the FTLE, we simulated considering step sizes $\ell = 10$, $\ell = 50$, $\ell = 200$ and $\ell = 1000$, and the results are the same.

3.2. Wolf linearization algorithm

In 1985, Wolf and coauthors proposed a method [32] for the calculation of Lyapunov exponents, which they defined as the *Lyapunov spectrum* of a dynamical system. Usually this method is used in time series analysis, but it can also be used to compute the dynamical evolution of mappings. To implement the Wolf Linearization Algorithm it is necessary to construct a set of linearized systems based on the mapping equations, in our case Eqs. (2)–(5). This procedure required an extensive algebra, since we have a four dimensional mapping for the stadium billiard with time dependent boundaries. The analytical results of the linearized systems can be found at the Appendix A.

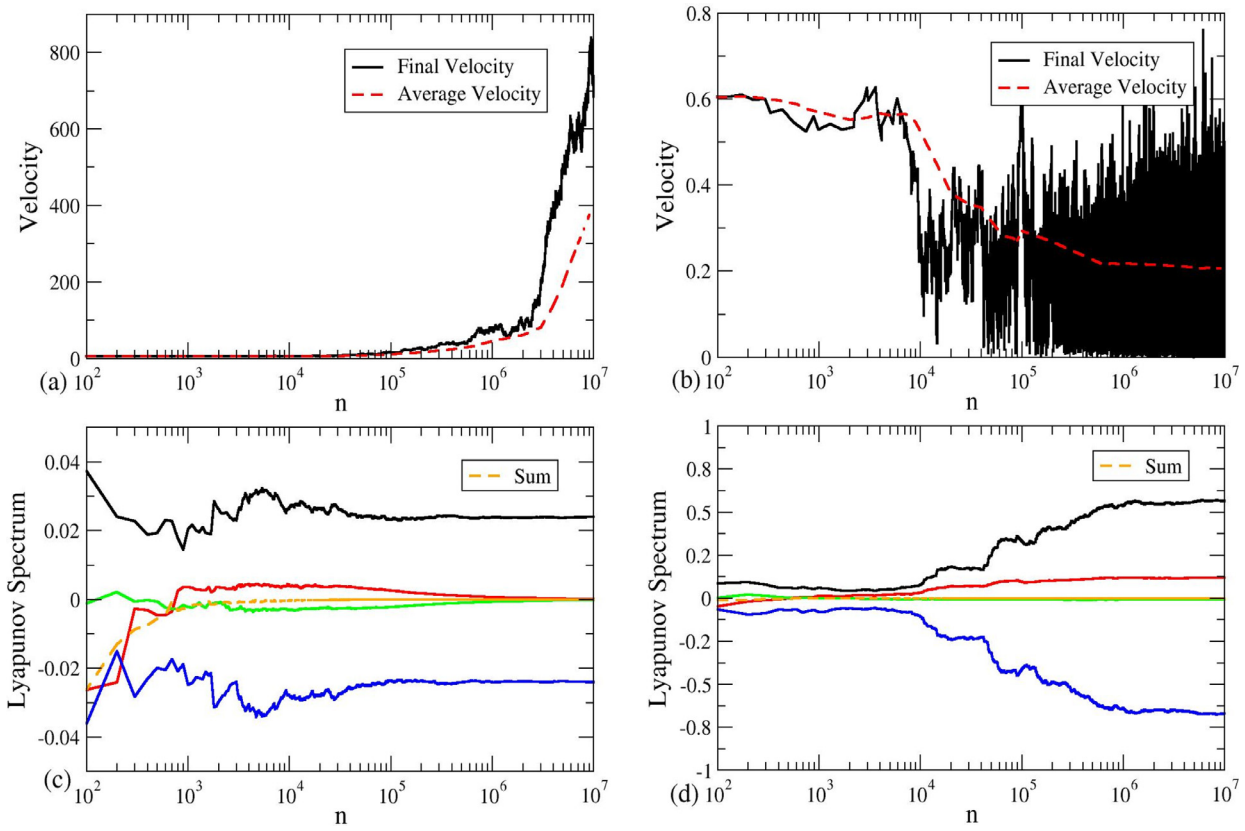

Fig. 4. Behaviour of the final and average velocity along with the Lyapunov spectrum, for both low and high ensembles, during 10^7 iterations of the time dependent stadium billiard. In (a) and (c) the high energy ensemble, with $V_0 = 6$, where the FA is inherent. Moreover, in (b) and (d) the low energy ensemble with $V_0 = 0.6$, where the decay of energy can be observed. The coloured curves shown in (c) and (d) correspond to the Lyapunov spectrum for the four dimensional system. The initial conditions were chosen along the chaotic sea.

As it is known in the literature [28], the resonance velocity divides high and low energy ensembles. Thus, the analysis of the Lyapunov spectrum should be done under both high energy ($V_0 > V_r$) and low energy ensemble ($V_0 < V_r$). Fig. 4 shows the difference between the ensembles.

Fig. 4 was constructed based on the results of the Wolf's Lyapunov spectrum algorithm for the dynamics of the time dependent stadium billiard. The parameters used were $l = 1$, $a = 0.5$, $b = 0.01$, and $m = 1$, the numerical value for the resonant velocity is $V_r \cong 1.2$. It is shown in Fig. 4(a) and (c) the high energy ensemble, for an initial velocity $V_0 = 6$. In (a) we see the velocity grows as a function of the number of collisions yielding in FA. The Lyapunov spectrum as a function of n is shown in (c). As expected for a non-dissipative system, the summation of the Lyapunov exponents, shown as the dashed orange line approaches zero for large enough n.

Considering now the initial velocity $V_0 = 0.6$ corresponding to the low energy ensemble, Fig. 4(b) and (d) show the behaviour of the velocity and the Lyapunov spectrum as a function of n. In (a), the final velocity V_{n+1}, given by Eq. (4) and the average velocity are decaying, characteristic of the time-dependent stadium billiard for $V_0 < V_r$. Moreover, in (d) the Lyapunov spectrum and its summation are shown as a function of n. As in the previous case, the summations also goes to zero for large n.

Furthermore, Fig. 4(c) and (d) show a change of behaviour right after 10^4 iterations. In Fig. 4(c) we observe FA and the fluctuations of the spectrum are ceased. While in Fig. 4(d) we have the changeover of the orbits behaviour, due to the "porous" invariant curves surrounding the KAM islands. In this case, we believe that after 10^4, this change over between chaos and quasi-regularity becomes more often in the dynamics.

Thus, after 10^4 iterations the system presents a dynamical change and at this time the behaviour of the velocity also changes. Additionally, that is when, for the high energy case the average velocity grows and, for the low energy case the average velocity decays. This dynamical change also affects the Lyapunov spectrum. The smooth behaviour for the Lyapunov exponents for long times, indicates that we do not have a "global change" in the dynamical scenario. After 10^4 iterations, the dynamical behaviour of the system does not change. For $V_0 > V_r$ we observe FA, while $V_0 < V_r$ we have decay of energy.

4. Final remarks

In the last few years, the study of the stadium-like billiard [25,28,29] has been revisited aiming to a better understanding of dynamical properties for different ensembles of energy. Such studies were the basis for this paper where we made an analysis of the Lyapunov exponents in order to describe the ensemble separation. The ensemble separation can be featured by the numerical values of the Lyapunov exponents. We used two different methods to evaluate the Lyapunov exponents for this system. Initially, we considered the finite time Lyapunov exponents where the distribution for the larger exponent shows a peak near the null value. Later, through the Wolf linearization algorithm, a full analysis of the Lyapunov spectrum lead to a consistent result. Quantitatively, we do have different results considering the values of Lyapunov exponents. However, qualitatively both methods show a good agreement regarding the separation of ensembles.

The Lyapunov spectrum and its distribution depends on the chosen ensemble of energies, leading to different dynamical scenarios. For the higher ensemble the FA rules the dynamics, while for the lower one, stickiness allied with the resonance lead the orbits to a steady state plateau for long times. In a near future, would be interesting to compare the exponent of the power-law decay, due to stickiness, in the recurrence time statistics between the high and low energy initial conditions. Additionally, investigate how we can compare the Lyapunov exponents using those both methods for other billiards and similar dynamical systems. This comparison might lead to more results concerning the complex and not yet fully understood interface between stickiness and FA.

Acknowledgements

MSP thanks to FAPESP (2012/00556-6) and FAPESP (2016/15127-4), ALPL acknowledges FAPESP (2014/25316-3) and FAPESP (2015/26699-6) for financial support. ILC thanks FAPESP (2011/19296-1) and EDL thanks FAPESP (2012/23688-5), (2017/14414-2) CNPq (303707/2015-1), Brazilian agencies. MPS and ALPL also thanks Professor Carl P. Dettmann for fruitful discussions and the University of Bristol during their visit. This research was supported by resources supplied by the Center for Scientific Computing (NCC/GridUNESP) of the São Paulo State University (UNESP). We also acknowledge the anonymous referee for contributions and important comments furnished in order to improve the paper.

Appendix A

This Appendix is devoted to the calculation of the linearized system for both cases of collisions. The linearized system is constructed by

$$\begin{pmatrix} \tilde{\phi} \\ \tilde{t} \\ \tilde{V} \\ \tilde{\alpha} \end{pmatrix} = J_S \begin{pmatrix} \phi \\ t \\ V \\ \alpha \end{pmatrix} \quad , \tag{A.1}$$

and

$$\begin{pmatrix} \tilde{\phi} \\ \tilde{t} \\ \tilde{V} \\ \tilde{\alpha} \end{pmatrix} = J_I \begin{pmatrix} \phi \\ t \\ V \\ \alpha \end{pmatrix} \quad , \tag{A.2}$$

where J_S is the Jacobian matrix for the successive collisions, and J_I the Jacobian matrix for the indirect ones.

The Jacobian matrix of the system is defined by

$$J = \begin{pmatrix} \frac{\partial \phi_{n+1}}{\partial \phi_n} & \frac{\partial \phi_{n+1}}{\partial t_n} & \frac{\partial \phi_{n+1}}{\partial V_n} & \frac{\partial \phi_{n+1}}{\partial \alpha_n} \\ \frac{\partial t_{n+1}}{\partial \phi_n} & \frac{\partial t_{n+1}}{\partial t_n} & \frac{\partial t_{n+1}}{\partial V_n} & \frac{\partial t_{n+1}}{\partial \alpha_n} \\ \frac{\partial V_{n+1}}{\partial \phi_n} & \frac{\partial V_{n+1}}{\partial t_n} & \frac{\partial V_{n+1}}{\partial V_n} & \frac{\partial V_{n+1}}{\partial \alpha_n} \\ \frac{\partial \alpha_{n+1}}{\partial \phi_n} & \frac{\partial \alpha_{n+1}}{\partial t_n} & \frac{\partial \alpha_{n+1}}{\partial V_n} & \frac{\partial \alpha_{n+1}}{\partial \alpha_n} \end{pmatrix} . \tag{A.3}$$

We consider first the successive collisions case, represented by the following equations

$$\begin{cases} \phi_{n+1} = \phi_n + \pi - 2\alpha_n \\ t_{n+1} = t_n + \dfrac{2R\cos(\alpha_n)}{V_n} \\ B_{n+1} = B_0\cos(wt_{n+1}) \\ \alpha_n^* = \alpha_n \\ V_{n+1} = \sqrt{V_n^2 + 4B_{n+1}^2 + 4V_nB_{n+1}\cos(\alpha_n^*)} \\ \alpha_{n+1} = \arcsin\left[\dfrac{|\vec{V_n}|}{|\vec{V_{n+1}}|}\sin(\alpha_n^*)\right] \end{cases} \tag{A.4}$$

Then the first line of the Jacobian matrix is given by

$$\frac{\partial\phi_{n+1}}{\partial\phi_n} = 1 \ ,$$
$$\frac{\partial\phi_{n+1}}{\partial t_n} = 0 \ ,$$
$$\frac{\partial\phi_{n+1}}{\partial V_n} = 0 \ ,$$
$$\frac{\partial\phi_{n+1}}{\partial\alpha_n} = -2 \ .$$

The second line is written as

$$\frac{\partial t_{n+1}}{\partial\phi_n} = 0 \ ,$$
$$\frac{\partial t_{n+1}}{\partial t_n} = 1 \ ,$$
$$\frac{\partial t_{n+1}}{\partial V_n} = \frac{-2R\cos(\alpha_n)}{V_n^2} = \frac{t_n - t_{n+1}}{V_n} \ ,$$
$$\frac{\partial t_{n+1}}{\partial\alpha_n} = \frac{-2R\sin(\alpha_n)}{V_n} = (t_n - t_{n+1})\tan(\alpha_n) \ .$$

To be able to continue with the derivatives, it is necessary to calculate also auxiliary derivatives for B_{n+1}, considering $w = 1$

$$\frac{\partial B_{n+1}}{\partial\phi_n} = 0 \ ,$$
$$\frac{\partial B_{n+1}}{\partial t_n} = -B_0\sin(t_{n+1}) \ ,$$
$$\frac{\partial B_{n+1}}{\partial V_n} = -B_0\sin(t_{n+1})\frac{\partial t_{n+1}}{\partial V_n} \ ,$$
$$\frac{\partial B_{n+1}}{\partial\alpha_n} = -B_0\sin(t_{n+1})\frac{\partial t_{n+1}}{\partial\alpha_n} \ .$$

The auxiliary derivatives for α_n^*

$$\frac{\partial\alpha_n^*}{\partial\phi_n} = 0 \ ,$$
$$\frac{\partial\alpha_n^*}{\partial t_n} = 0 \ ,$$
$$\frac{\partial\alpha_n^*}{\partial V_n} = 0 \ ,$$
$$\frac{\partial\alpha_n^*}{\partial\alpha_n} = 1 \ .$$

Hence, the third line is given by

$$\frac{\partial V_{n+1}}{\partial\phi_n} = 0 \ ,$$
$$\frac{\partial V_{n+1}}{\partial t_n} = \frac{1}{V_{n+1}}\left[2V_n\cos(\alpha_n^*)\frac{\partial B_{n+1}}{\partial t_n} + 4B_{n+1}\frac{\partial B_{n+1}}{\partial t_n}\right] ,$$

$$\frac{\partial V_{n+1}}{\partial V_n} = \frac{1}{V_{n+1}}\left[V_n + 2B_{n+1}\cos(\alpha_n^*) + 2V_n\cos(\alpha_n^*)\frac{\partial B_{n+1}}{\partial V_n} + 4B_{n+1}\frac{\partial B_{n+1}}{\partial V_n}\right],$$

$$\frac{\partial V_{n+1}}{\partial \alpha_n} = \frac{1}{V_{n+1}}\left[2V_n\cos(\alpha_n^*)\frac{\partial B_{n+1}}{\partial \alpha_n} - 2B_{n+1}V_n\sin(\alpha_n^*) + 4B_{n+1}\frac{\partial B_{n+1}}{\partial \alpha_n}\right].$$

Finally, the fourth line is calculated by

$$\frac{\partial \alpha_{n+1}}{\partial \phi_n} = 0\ ,$$

$$\frac{\partial \alpha_{n+1}}{\partial t_n} = \frac{1}{V_{n+1}^2\cos(\alpha_{n+1})}\left[-V_n\sin(\alpha_n^*)\frac{\partial V_{n+1}}{\partial t_n}\right],$$

$$\frac{\partial \alpha_{n+1}}{\partial V_n} = \frac{1}{V_{n+1}^2\cos(\alpha_{n+1})}\left[\sin(\alpha_n^*)V_{n+1} - V_n\sin(\alpha_n^*)\frac{\partial V_{n+1}}{\partial V_n}\right],$$

$$\frac{\partial \alpha_{n+1}}{\partial \alpha_n} = \frac{1}{V_{n+1}^2\cos(\alpha_{n+1})}\left[V_n\cos(\alpha_n^*)V_{n+1} - V_n\sin(\alpha_n^*)\frac{\partial V_{n+1}}{\partial \alpha_n}\right].$$

Now we consider the other type of collisions, the indirect case, represented by the following equations

$$\begin{cases} \psi_n = \alpha_n - \phi_n \\ \alpha_n^* = \arcsin\left[2\sin(\psi_n)\cos(\Phi) - \sin\alpha_n - \dfrac{l\sin\psi_n}{R}\right] \\ \phi_{n+1} = \psi_n - \alpha_n^* \\ t_{n+1} = t_n + \dfrac{R[\cos(\phi_n) + \cos(\phi_{n+1}) - 2\cos(\Phi)] + l}{V_n\cos(\psi_n)} \\ B_{n+1} = B_0\cos(wt_{n+1}) \\ V_{n+1} = \sqrt{V_n^2 + 4B_{n+1}^2 + 4V_nB_{n+1}\cos(\alpha_n^*)} \\ \alpha_{n+1} = \arcsin\left[\dfrac{|\vec{V_n}|}{|\vec{V_{n+1}}|}\sin(\alpha_n^*)\right] \end{cases} \tag{A.5}$$

At first, it is necessary to do some auxiliary derivatives, so for ψ_n

$$\frac{\partial \psi_n}{\partial \phi_n} = -1\ ,$$

$$\frac{\partial \psi_n}{\partial t_n} = 0\ ,$$

$$\frac{\partial \psi_n}{\partial V_n} = 0\ ,$$

$$\frac{\partial \psi_n}{\partial \alpha_n} = 1\ ,$$

and for α_n^*

$$\frac{\partial \alpha_n^*}{\partial \phi_n} = \frac{1}{\cos(\alpha_n^*)}\left[-2\cos(\psi_n)\cos(\Phi) + \frac{l\cos(\psi_n)}{R}\right],$$

$$\frac{\partial \alpha_n^*}{\partial t_n} = 0\ ,$$

$$\frac{\partial \alpha_n^*}{\partial V_n} = 0\ ,$$

$$\frac{\partial \alpha_n^*}{\partial \alpha_n} = \frac{1}{\cos(\alpha_n^*)}\left[2\cos(\psi_n)\cos(\Phi) - \cos(\alpha_n) - \frac{l\cos(\psi_n)}{R}\right].$$

Thus, the first line of the Jacobian matrix J_I is calculated by

$$\frac{\partial \phi_{n+1}}{\partial \phi_n} = -1 - \frac{\partial \alpha_n^*}{\partial \phi_n},$$
$$\frac{\partial \phi_{n+1}}{\partial t_n} = 0,$$
$$\frac{\partial \phi_{n+1}}{\partial V_n} = 0,$$
$$\frac{\partial \phi_{n+1}}{\partial \alpha_n} = 1 - \frac{\partial \alpha_n^*}{\partial \alpha_n}.$$

The second line is

$$\frac{\partial t_{n+1}}{\partial \phi_n} = (t_n - t_{n+1})\tan(\psi_n) - \frac{R}{V_n\cos(\psi_n)}\left[\sin(\phi_n) + \sin(\phi_{n+1})\frac{\partial \phi_{n+1}}{\partial \phi_n}\right],$$
$$\frac{\partial t_{n+1}}{\partial t_n} = 1,$$
$$\frac{\partial t_{n+1}}{\partial V_n} = \frac{t_n - t_{n+1}}{V_n},$$
$$\frac{\partial t_{n+1}}{\partial \alpha_n} = -(t_n - t_{n+1})\tan(\psi_n) - \frac{R}{V_n\cos(\psi_n)}\left[\sin(\phi_{n+1})\frac{\partial \phi_{n+1}}{\partial \alpha_n}\right].$$

Furthermore, the auxiliary derivatives for B_{n+1}, considering $w = 1$ are written as

$$\frac{\partial B_{n+1}}{\partial \phi_n} = -B_0 \sin t_{n+1}\frac{\partial t_{n+1}}{\partial \phi_n},$$
$$\frac{\partial B_{n+1}}{\partial t_n} = -B_0 \sin t_{n+1},$$
$$\frac{\partial B_{n+1}}{\partial V_n} = -B_0 \sin t_{n+1}\frac{\partial t_{n+1}}{\partial V_n},$$
$$\frac{\partial B_{n+1}}{\partial \alpha_n} = -B_0 \sin t_{n+1}\frac{\partial t_{n+1}}{\partial \alpha_n}.$$

The third line is calculated by

$$\frac{\partial V_{n+1}}{\partial \phi_n} = \frac{1}{V_{n+1}}\left[2V_n\cos(\alpha_n^*)\frac{\partial B_{n+1}}{\partial \phi_n} - 2B_{n+1}V_n\sin(\alpha_n^*)\frac{\partial \alpha_n^*}{\partial \phi_n} + 4B_{n+1}\frac{\partial B_{n+1}}{\partial \alpha_n}\right],$$
$$\frac{\partial V_{n+1}}{\partial t_n} = \frac{1}{V_{n+1}}\left[2V_n\cos(\alpha_n^*)\frac{\partial B_{n+1}}{\partial t_n} + 4B_{n+1}\frac{\partial B_{n+1}}{\partial t_n}\right],$$
$$\frac{\partial V_{n+1}}{\partial V_n} = \frac{1}{V_{n+1}}\left[V_n + 2B_{n+1}\cos(\alpha_n^*) + 2V_n\cos(\alpha_n^*)\frac{\partial B_{n+1}}{\partial V_n} + 4B_{n+1}\frac{\partial B_{n+1}}{\partial V_n}\right],$$
$$\frac{\partial V_{n+1}}{\partial \alpha_n} = \frac{1}{V_{n+1}}\left[2V_n\cos(\alpha_n^*)\frac{\partial B_{n+1}}{\partial \alpha_n} - 2B_{n+1}V_n\sin(\alpha_n^*)\frac{\partial \alpha_n^*}{\partial \alpha_n} + 4B_{n+1}\frac{\partial B_{n+1}}{\partial \alpha_n}\right].$$

Finally, the fourth line of J_I is

$$\frac{\partial \alpha_{n+1}}{\partial \phi_n} = \frac{1}{V_{n+1}^2 \cos(\alpha_{n+1})}\left[V_n \cos(\alpha_n^*)\frac{\partial \alpha_n^*}{\partial \phi_n}V_{n+1} - V_n \sin(\alpha_n^*)\frac{\partial V_{n+1}}{\partial \phi_n}\right],$$

$$\frac{\partial \alpha_{n+1}}{\partial t_n} = \frac{1}{V_{n+1}^2 \cos(\alpha_{n+1})}\left[-V_n \sin(\alpha_n^*)\frac{\partial V_{n+1}}{\partial t_n}\right],$$

$$\frac{\partial \alpha_{n+1}}{\partial V_n} = \frac{1}{V_{n+1}^2 \cos(\alpha_{n+1})}\left[\sin(\alpha_n^*)V_{n+1} - V_n \sin(\alpha_n^*)\frac{\partial V_{n+1}}{\partial V_n}\right],$$

$$\frac{\partial \alpha_{n+1}}{\partial \alpha_n} = \frac{1}{V_{n+1}^2 \cos(\alpha_{n+1})}\left[V_n \cos(\alpha_n^*)\frac{\partial \alpha_n^*}{\partial \alpha_n}V_{n+1} - V_n \sin(\alpha_n^*)\frac{\partial V_{n+1}}{\partial \alpha_n}\right].$$

References

[1] Hilborn RC. Chaos and nonlinear dynamics: an introduction for scientists and engineers. Oxford University Press; 1994.
[2] Lichtenberg AJ, Lieberman MA. Regular and chaotic dynamics. Appl. math. sci. 38. Springer Verlag; 1992.
[3] Zaslasvsky GM. Physics of chaos in Hamiltonian systems. Imperial College Press; 2007.
[4] Zaslasvsky GM. Hamiltonian chaos and fractional dynamics. Oxford University Press; 2008.
[5] Altmann EG, Portela JSE, Tél T. Rev Mod Phys 2013;85:869.
[6] Meiss JD. Chaos 2015;25:097602.
[7] Livorati AL, Kroetz T, Dettmann CP, Caldas IL, Leonel ED. Phys Rev E 2012;86:036203.
[8] Leine RI, Nijmeijer H. Dynamics and bifurcations of non-Smooth mechanical systems, vol. 18. Springer Science & Business; 2013.
[9] Bonatto C, Garreau JC, Gallas JAC. Phys Rev Lett 2005;95:143905.
[10] Grebogi C, Ott E, Yorke JA. Phys Rev Lett 1982;48:1507.
[11] Birkhoff GD. Dynamical systems. American Mathematical Society; 1927.
[12] Sinai YG. Rus Math Surv 1970;25:137.
[13] Bunimovich LA. Commun Math Phys 1979;65:295.
[14] Bunimovich LA, Sinai YG. Commun Math Phys 1981;78:479.
[15] Gallavotti G, Ornstein DS. Commun Math Phys 1974;38:83.
[16] Friedman N, et al. Phys Rev Lett 2001;86:1518.
[17] Stokmann HJ. Quantum chaos: an introduction. Cambridge University Press; 1999.
[18] Marcus CM, et al. Phys Rev Lett 1992;69:506.
[19] Fré P, Sorin AS. J High Energy Phys 2010;3:1.
[20] Stone AD. Nature 2010;465:696.
[21] Bunimovich LA. Funct Anal Appl 1974;8:73.
[22] Loskutov A, Ryabov AB, Akinshin LG. J Exp Theor Phys 1999;89:966.
[23] Livorati ALP, Loskutov A, Leonel ED. J Phys A 2011;44:175102.
[24] Loskutov A, Ryabov A. J Stat Phys 2002;108:995.
[25] Loskutov A, Ryabov AB, Leonel ED. Physica A 2010;389:5408.
[26] Loskutov A, Ryabov AB, Akinshin LG. J Phys A 2000;33:7973.
[27] Fermi E. Phys Rev 1949;75:1169.
[28] Livorati ALP, Palmero MS, Dettmann CP, Caldas IL, Leonel ED. J Phys A 2014;47:365101.
[29] Livorati ALP, Loskutov A, Leonel ED. Physica A 2012;391:4756.
[30] Szezech JDJ, Lopes SR, Viana RL. Phys Lett A 2005;335:394.
[31] Manchein C, Beims MW, Rost JM. Physica A 2014;400:186.
[32] Wolf A, Swift JB, Swinney HL, Vastano JA. Psysica D 1985;285:16.
[33] Chernov N, Markarian R. Chaotic billiards. American Mathematical Society; 2006.
[34] Karlis AK, Papachristou PK, Diakonos FK, Constantoudis V, Schmelcher P. Phys Rev Lett 2006;97:194102.
[35] Lenz F, Diakonos FK, Schmelcher P. Phys Rev Lett 2008;100:014103.
[36] Lenz F, Petri C, Koch FRN, Diakonos FK, Schmelcher P. New J Phys 2009;11:083035.
[37] Leonel ED, Bunimovich LA. Phys Rev Lett 2010;104:224101.
[38] Benettin G, Galgani L, Giorgilli A, Streleyn JM. Meccanica 1980;15:9.
[39] Silva RD, Manchein C, Beims M, Altmann E. Phys Rev E 2015;91:062907.